gene than for its wild-type chromosomal version (*14*). Extrinsic and intrinsic noise must be combined to explain the observed amount of variation; regulatory mechanisms aimed at suppressing noise, such as negative feedback (*15*), need to respond to both sources.

To be able to model the behavior of transcriptional regulatory circuits, it is essential to understand the interplay between regulatory dynamics and noise. We introduced a synthetic oscillatory network, termed the Repressilator (*7, 16*), into strain M22 (Table 1 and Fig. 2F). This network causes periodic synthesis of LacI, which repeatedly turns both promoters on and off. Large excursions in overall fluorescence intensity occur (high η_{tot}). An additional consequence is significant increases in η_{int} (compared with that in a similar strain with the same mean rate of transcription; see Table 1). This is consistent with theoretical predictions that noise is greater during the approach to, rather than at, a steady state (*17*). Thus, regulatory dynamics can cause substantial changes in noise levels.

If the amount of noisiness in a cell is genetically determined, then different strains might exhibit different basal noise levels (both intrinsic and extrinsic). Therefore, we inserted the two reporter genes in various genetic backgrounds. The amount of noise was similar in most strains, but one, D22, displayed about twice the amount of noise (Fig. 3, B and C, and Table 1). The known genotype of this strain differed from that of a related, less noisy, strain only by deletion of the *recA* gene, which suggests that lack of RecA was responsible for the increased noise. In agreement with this hypothesis, transduction of the Δ*recA* allele into less noisy strains such as M22, JM22, and RP22 was sufficient to substantially increase η_{int} (Fig. 2, B and C, and Table 1). This increased noise in Δ*recA* cells does not depend on a loss of viability (*18*). RecA acts to rescue stalled replication forks (*19*), which suggests that increased noise may arise from transient copy-number differences between different parts of the chromosome.

These results show that intrinsic and extrinsic classes of noise are important in setting cell-cell variation in gene expression. Both types of noise should similarly occur in all other intracellular reactions involving small numbers of reactants. Any cellular component that suffers intrinsic fluctuations in its own concentration will act as a source of extrinsic noise for other components with which it interacts. Thus, given the substantial noise measured here, reliable functioning of the cell may require genetic networks that suppress, or are robust to, fluctuations (*15, 20*). At the same time, it is clear that noise, if amplified, offers the opportunity to generate long-term heterogeneity in a clonal population.

References and Notes

1. P. Guptasarma, *Bioessays* **17**, 987 (1995).
2. J. L. Spudich *et al.*, *Nature* **262**, 467 (1976).
3. H. H. McAdams *et al.*, *Proc. Natl. Acad. Sci. U.S.A.* **94**, 814 (1997).
4. P. Heitzler *et al.*, *Cell* **64**, 1083 (1991).
5. M. S. Ko, *Bioessays* **14**, 341 (1992).
6. S. Fiering *et al.*, *Bioessays* **22**, 381 (2000).
7. See supporting data on *Science* Online.
8. P. S. Swain *et al.*, *Proc. Natl. Acad. Sci. U.S.A.*, in press.
9. R. Lutz *et al.*, *Nucleic Acids Res.* **25**, 1203 (1997).
10. U. Deuschle *et al.*, *EMBO J.* **5**, 2987 (1986).
11. P. C. Maloney, B. Rotman, *J. Mol. Biol.* **73**, 77 (1973).
12. J. Paulsson, M. Ehrenberg, *Q. Rev. Biophys.* **34**, 1 (2001).
13. At high IPTG concentrations, cells are fully induced, regardless of the amount of LacI they contain, whereas at low IPTG concentrations they are uniformly repressed. In both cases, LacI fluctuations are buffered (by excess IPTG or excess LacI, respectively), and hence η_{ext} must be small. However, between these two extremes, fluctuations in the amount of LacI cause corresponding fluctuations in the transcription rate of the reporter genes, and thus η_{ext} reaches a maximum value. See (*8*) for a more detailed treatment.
14. D. Boyd, *et al.*, *J. Bacteriol.* **182**, 842 (2000).
15. A. Becskei, L. Serrano, *Nature* **405**, 590 (2000).
16. M. B. Elowitz, S. Leibler, *Nature* **403**, 335 (2000).
17. M. Thattai, A. van Oudenaarden, *Proc. Natl. Acad. Sci. U.S.A.* **98**, 8614 (2001).
18. Deletion of *recA* has pleiotropic effects, including an increased fraction of nonviable cells in growing cultures (*21*). By following microcolony formation with time-lapse microscopy (*7*), we checked whether the observed noise increase in Δ*recA* populations could be attributed to a subpopulation of nonviable cells. All M22 (*recA*$^+$) cells measured formed microcolonies (10 of 10), whereas some (2 of 14) of the M22 Δ*recA* cells did not. In both cases, noise levels of viable cells at the initial timepoint were consistent with those previously obtained with larger samples.
19. M. M. Cox *et al.*, *Nature* **404**, 37 (2000).
20. U. Alon *et al.*, *Nature* **397**, 168 (1999).
21. F. N. Capaldo, S. D. Barbour, *Basic Life Sci.* **5A**, 405 (1975).
22. M. J. Casadaban, *J. Mol. Biol.* **104**, 541 (1976).
23. D. Yu *et al.*, *Proc. Natl. Acad. Sci. U.S.A.* **97**, 5978 (2000).
24. J. S. Parkinson, S. E. Houts, *J. Bacteriol.* **151**, 106 (1982).
25. B. J. Meyer, R. Maurer, M. Ptashne, *J. Mol. Biol.* **139**, 163 (1980).
26. J. B. Andersen *et al.*, *Appl. Environ. Microbiol.* **64**, 2240 (1998).

27. We thank U. Alon, S. Bekiranov, J. Dworkin, D. Endy, C. Guet, R. Kishony, S. Leibler, D. O'Carroll, N. Rajewsky, B. Shraiman, D. Thaler, and especially M. G. Surette for conversations and suggestions; A. Teresky and the Levine Lab for help; and J. Paulsson for his suggestion about the extrinsic noise profile. Recombination-proficient strains were provided by D. Court. Supported by the Burroughs-Wellcome Fund and the Seaver Institute (M.B.E.) and by NIH grant GM59018 (P.S.S.).

Supporting Online Material

www.sciencemag.org/cgi/content/full/297/5584/1183/DC1
Materials and Methods
Fig. S1

14 February 2002; accepted 13 June 2002

S-Nitrosylation of Matrix Metalloproteinases: Signaling Pathway to Neuronal Cell Death

Zezong Gu,[1] Marcus Kaul,[1] Boxu Yan,[2]* Steven J. Kridel,[2]* Jiankun Cui,[1] Alex Strongin,[2] Jeffrey W. Smith,[2] Robert C. Liddington,[2] Stuart A. Lipton[1]†

Matrix metalloproteinases (MMPs) are implicated in the pathogenesis of neurodegenerative diseases and stroke. However, the mechanism of MMP activation remains unclear. We report that MMP activation involves S-nitrosylation. During cerebral ischemia in vivo, MMP-9 colocalized with neuronal nitric oxide synthase. S-Nitrosylation activated MMP-9 in vitro and induced neuronal apoptosis. Mass spectrometry identified the active derivative of MMP-9, both in vitro and in vivo, as a stable sulfinic or sulfonic acid, whose formation was triggered by S-nitrosylation. These findings suggest a potential extracellular proteolysis pathway to neuronal cell death in which S-nitrosylation activates MMPs, and further oxidation results in a stable posttranslational modification with pathological activity.

Matrix metalloproteinases (MMPs) constitute a family of extracellular soluble or membrane-bound proteases that are involved in remodeling extracellular matrix. A role for MMPs has also been suggested in the pathogenesis of both acute and chronic neurodegenerative disorders such as stroke, Alzheimer's disease, HIV-associated dementia, and multiple sclerosis (*1–3*). MMP-9 in particular is elevated in human stroke (*4*). Mice treated with MMP inhibitors or deficient in MMP-9 manifest reduced cerebral infarct size (*5–7*). Members of the MMP family (with the exception of MMP-7) share structural features including propeptide, catalytic, and hemopexin domains. One cysteine residue in

[1]Center for Neuroscience and Aging, [2]Program in Cell Adhesion and Extracellular Matrix Biology, The Burnham Institute, 10901 North Torrey Pines Road, La Jolla, CA 92037, USA.

*These authors contributed equally to this work.
†To whom correspondence should be addressed. E-mail: slipton@burnham.org

the conserved autoinhibitory region of the propeptide domain coordinates a zinc ion (Zn^{2+}) in the catalytic site and thus inhibits the proform of the enzyme. Disruption of the Zn^{2+}-cysteine interaction exposes Zn^{2+} in the active site, allowing H_2O to bind, and consequently activates the MMP zymogen by a mechanism known as the cysteine switch (*8*, *9*). Under physiological conditions, MMP activity is also controlled by tissue inhibitors of MMPs (TIMPs) (*1*, *2*).

Nitric oxide (NO) is a signaling molecule that regulates many biological processes in the nervous system, including neurotransmitter release, plasticity, and apoptosis (*10*–*12*). The chemical reactions of NO are largely dictated by its redox state (*13*). NO can modulate the biological activity of many proteins by reacting with cysteine thiol to form an S-nitrosylated derivative (*14*–*17*). Cerebral ischemia and reperfusion result in nitrosative and oxidative stress, and hence the production of NO and reactive oxygen species (*18*, *19*). The regulation of protein function by S-nitrosylation has led to the proposal that nitrosothiols function as posttranslational modifications analogous to phosphorylation or acetylation. Although the factors governing cysteine reactivity toward nitrosylating agents are not completely understood, critical features include basic and acidic residues flanking the reactive cysteine, either in linear sequence or as a consequence of the three-dimensional organization of the protein, which catalyze the nitrosylation and denitrosylation steps (*20*). Because such a motif exists in MMPs, we sought to determine whether S-nitrosylation could mechanistically trigger the cysteine switch to activate MMPs under pathophysiologically relevant conditions.

Gelatin zymography revealed an increase in both the expression of proMMP-9 and in MMP-9 activity in the ischemic hemisphere of rodents after focal cerebral ischemia and reperfusion (Fig. 1A). The slight decrease in actin in the damaged hemisphere may reflect cell loss. MMP-2 was not activated (*21*). Similar changes in MMP-9 have recently been reported after human embolic stroke (*4*). MMP activity was particularly elevated in ischemic brain parenchyma after ischemia and reperfusion (Fig. 1B). Moreover, activation of MMP was abrogated after stroke in neuronal nitric oxide synthase (nNOS) knockout mice or in wild-type animals that had been treated with the relatively specific nNOS inhibitor 3-bromo-7-nitroindazole (3br7NI) (Fig. 1B). Neuroprotection has been demonstrated previously under each of these conditions of NOS inhibition (*21*, *22*). In wild-type animals not treated with NOS inhibitors, immunocytochemistry revealed that many neurons in ischemic cortex manifested MMP activity (Fig. 1C, arrows). We also observed substantial colocalization of MMP-9 and nNOS in the ischemic cortex (Fig. 1D). Hence, there is coincident production of NO and MMP-9 activity after ischemia and reperfusion.

To determine whether MMP-9 could be S-

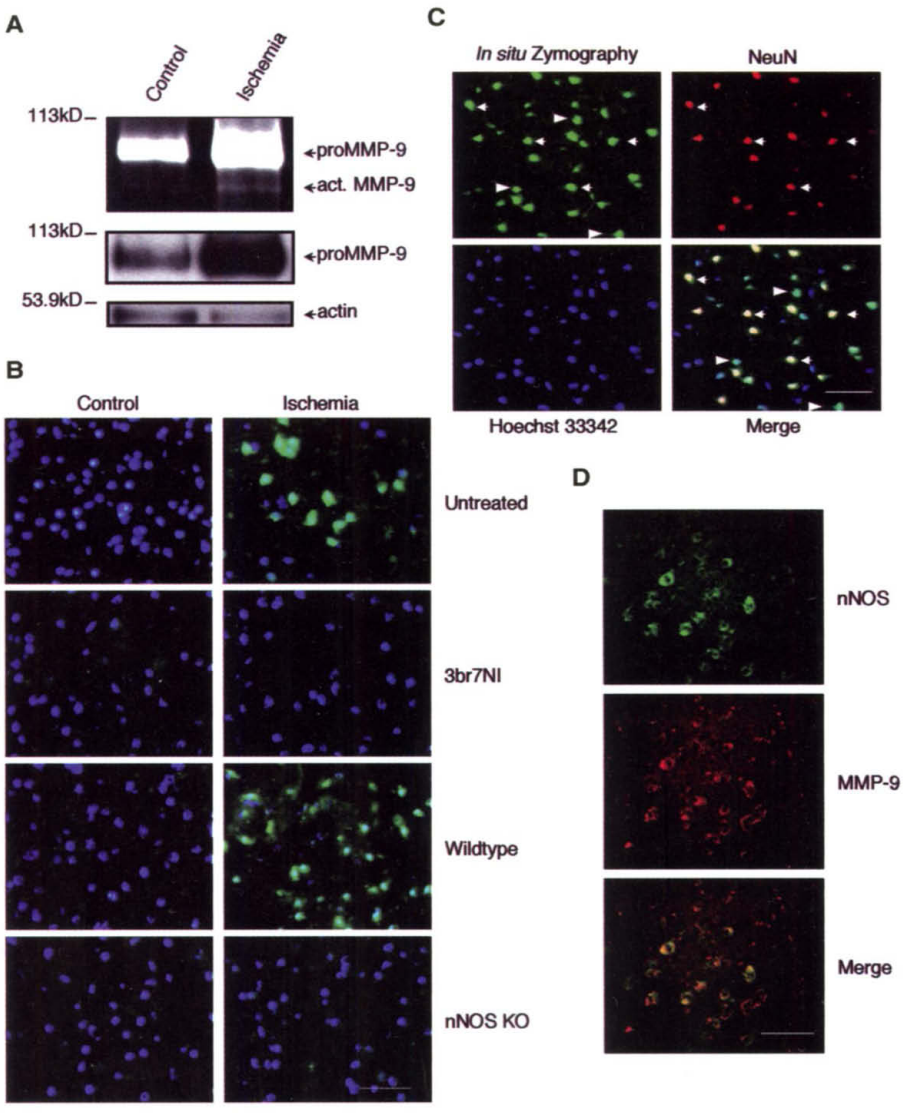

Fig. 1. nNOS-associated MMP-9 activation in ischemic cortex after middle cerebral artery (MCA) ischemia and reperfusion. (**A**) (Top) Gelatin zymography showing increased proMMP-9 expression and MMP-9 activity on the ischemic side of the brain compared with the contralateral side after 2-hour MCA occlusion and 24-hour reperfusion in C57BL/6J mice ($n = 7$). (Middle) Immunoblotting with antibody to MMP-9, showing increased MMP-9 expression on the ischemic side of the mouse brain compared with the control side. (Bottom) A slight decrease in actin on the ischemic side of the brain may reflect cell loss. The right MCA was occluded by intraluminal filament for 2 hours and then removed for reperfusion (*28*). MMP-9 was extracted from brain tissue in tris buffer [50 mM tris (pH 7.6), 5 mM $CaCl_2$, 150 mM NaCl, 0.05% Brij35] containing 1% Triton X-100, followed by affinity precipitation with gelatin Sepharose 4B (*29*). (**B**) In situ zymography with the MMP fluorogenic substrate DQ-gelatin-FITC (Molecular Probes) was performed on fresh cryostat sections of mouse brains harvested after MCA ischemia and reperfusion. Deconvolution microscopy revealed increased MMP activity (green) in the ischemic cortex relative to the control side (untreated, C57BL/6J). Counterstaining with Hoechst 33342 (blue) showed decreased nuclear DNA staining, indicating cell loss in the ischemic cortex after ischemia and reperfusion. Increased MMP activity in the ischemic cortex was abrogated in mice injected intraperitoneally before ischemia with 3-bromo-7-nitroindazole (3br7NI, 30 mg per kg of body weight) (Alexis Biochemicals, San Diego; control contained soybean oil vehicle) and in nNOS knockout (KO) mice (Jackson Laboratory, Bar Harbor, ME) but not in wild-type control mice. (**C**) Neurons (red, NeuN immunopositive) double labeled for MMP activity (green, arrows) in the ischemic cortex. Nuclear DNA was visualized by staining with Hoechst 33342 (blue). Some nonneuronal cells also showed MMP activity (arrowheads). (**D**) Colocalizaton (yellow) of nNOS (green) and MMP-9 (red) in the ischemic cortex was detected by double immunofluorescent staining after MCA ischemia and reperfusion. Scale bars, 50 μm.

nitrosylated and thus activated by NO in vitro, we generated a recombinant proMMP-9 that included the propeptide and catalytic domains of MMP-9 (R-proMMP-9). To eliminate the effects of TIMP-1 binding, which might interfere with catalysis and activation of MMP-9, we did not include the hemopexin domain. We incubated R-proMMP-9, purified from conditioned medium of stably transfected human embryonic kidney 293 (HEK293) cells (*23*), with the physiological NO donor *S*-nitrosocysteine (SNOC). We detected *S*-nitrosothiol generation by measuring the fluorescent compound 2,3-naphthyltriazole (NAT) (*24*). NAT is stoichiometrically converted from 2,3-diaminonaphthalene (DAN) by NO released from S-nitrosylated proteins and thus provides a quantitative measure of *S*-nitrosothiol formation. SNOC-treated R-proMMP-9 resulted in significant *S*-nitrosothiol formation (Fig. 2A). To ensure that the *S*-nitrosothiol generated under these conditions represented *S*-nitroso-MMP-9 and not residual SNOC, we examined the stability of *S*-nitrosothiols at different incubation times. The S-nitrosylation product of SNOC-treated R-proMMP-9 was much more stable than SNOC alone; within 15 min of incubation, more than 95% of the SNOC had decayed, whereas more than 80% of the *S*-nitroso-MMP-9 remained (fig. S1) (*24*). This temporal separation allowed us to distinguish SNOC from *S*-nitroso-MMP-9 in the fluorescent *S*-nitrosothiol assay.

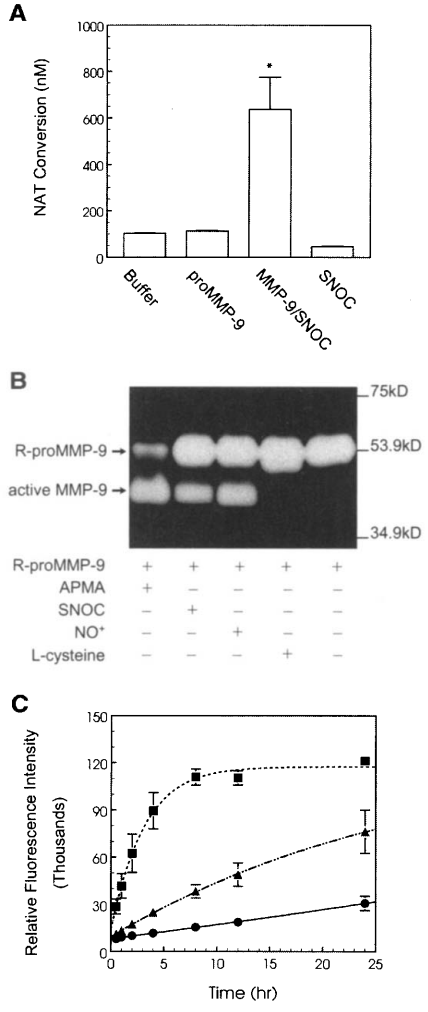

Fig. 2. S-Nitrosylation and consequent activation of MMP-9 in vitro by SNOC. **(A)** R-proMMP-9 (1.1 mg/ml) was incubated with SNOC (200 μM) for 15 min at room temperature. S-Nitrosylated MMP-9 thus generated was assessed by release of NO, causing the conversion of DAN to the fluorescent compound NAT (*$P < 0.03$ by analysis of variance). SNOC itself quickly decayed and thus resulted in insignificant *S*-nitrosothiol readings in this assay (see also fig. S1) (*24*). **(B)** Activation of proMMP-9 by APMA, SNOC, and acidified sodium nitrite (to yield nitrosonium, NO^+). R-proMMP-9 (100 ng/ml) was reacted with 200 μM APMA, SNOC, acidified sodium nitrite, or L-cysteine for 18 hours at room temperature and then analyzed by gelatin zymography. SNOC was generated by reaction of sodium nitrite and L-cysteine as described (*30*). The digested matrix, revealed by staining with Coomassie blue, indicated proteolytic activity. **(C)** Kinetics of activation of R-proMMP-9 treated with APMA (■) SNOC (▲) or untreated control (●). MMP activity was assessed by the cleavage rate of fluorogenic substrate I peptide (25 μM; Calbiochem, San Diego, CA; excitation wavelength, 280 ± 1 nm; emission wavelength, 360 ± 5 nm).

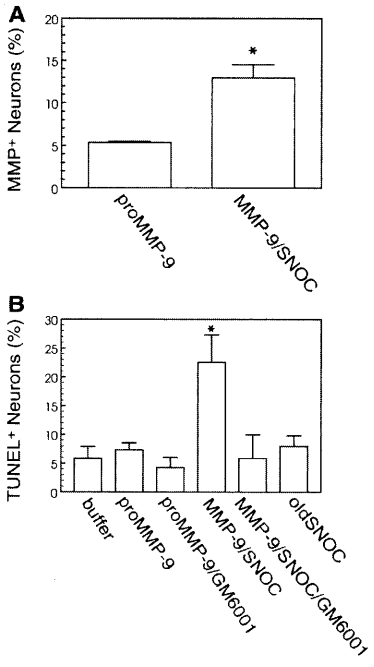

Fig. 3. Exogenous MMP-9 activated by SNOC induces neuronal apoptosis in cerebrocortical cell culture. **(A)** The percentage of MAP-2-positive neurons displaying MMP activity increased after exposure to ~150 pM proMMP-9 that had been preactivated with 200 μM SNOC (*$P <$ 0.01 by Student's t test; n = 1500 neurons counted in five separate experiments) (*24*). **(B)** Quantification of neuronal apoptosis induced by R-proMMP-9 preactivated by SNOC before addition to cerebrocortical cultures for 18 hours. SNOC-activated MMP-9 significantly increased neuronal apoptosis, whereas the MMP inhibitor GM6001 abrogated the effect (*$P <$ 0.01 by analysis of variance; n = 4000 neurons scored in six experiments). NO was dissipated from old SNOC by overnight incubation before addition.

To determine whether S-nitrosylation of R-proMMP-9 resulted in its activation, we compared the effects of the exogenous MMP-9 activator *p*-aminophenylmercuric acetate (APMA) with those of SNOC and another nitrosylating agent, acidified sodium nitrite. Incubation with APMA, SNOC, or acidified sodium nitrite led to a partial conversion of the 53.5-kD R-proMMP-9 into the 41.2-kD activated form of MMP-9 (Fig. 2B); we confirmed the respective masses by mass spectrometry (*21*). Activation was inhibited in the presence of the MMP-specific hydroxamate inhibitor GM6001 (*21*). We then compared the activity of R-proMMP-9 incubated with APMA or SNOC by assaying the ability to cleave a synthetic peptide substrate (Fig. 2C). The initial velocity of R-proMMP-9 activation was 4.80 μM/hour by APMA compared with 0.88 μM/hour by SNOC. S-Nitrosylation led to similar activation of the full-length MMP-9 as well (fig. S2) (*24*). These findings demonstrate that MMP-9 can undergo S-nitrosylation in vitro and show that NO can directly activate MMP-9.

We examined the effects of NO-activated MMP-9 on neuronal cell apoptosis in cerebrocortical cultures. The percentage of neurons exhibiting MMP activity increased after exposure to R-proMMP-9 that had been preactivated with SNOC, compared with R-proMMP-9 alone (Fig. 3A and fig. S3A) (*24*). SNOC from which NO was dissipated did not activate R-proMMP-9 and did not increase the percentage of neurons exhibiting MMP activity (*21*). Additionally, 18 hours after exposing neurons to SNOC-activated R-proMMP-9, we scored apoptotic neurons by staining with the neuronal marker anti–microtubule-associated protein–2 (MAP-2) and terminal deoxynucleotidyltransferase-mediated deoxyuridine triphosphate nick-end labeling (TUNEL) in conjunction with condensed nuclear morphology assessed with Hoechst 33342 (fig. S3B) (*24*). For these experiments, R-proMMP-9 was preactivated by SNOC; NO had already been released from SNOC by the time the cultures were incubated with the activated MMP-9, as determined by measurement with an NO-sensitive electrode (*11*). Hence, direct release of NO from SNOC or the formation of peroxynitrite ($ONOO^-$) due to the release of NO from SNOC and subsequent reaction with superoxide anion (O_2^-) could not have accounted for the observed neuronal apoptosis (*11*). Treatment of neurons with NO-activated MMP-9 increased apoptosis, whereas treatment with the MMP inhibitor GM6001 blocked neuronal cell death (Fig. 3B). We

also observed that many neurons became detached from the dish after exposure to NO-activated MMP-9. These results strongly suggest that even high levels of inactivated proMMP-9 protein do not have a deleterious effect on neurons. However, activation of MMP-9 by NO has toxic effects.

Although *S*-nitroso-MMP-9 formation was associated with MMP-9 activation, nitrosothiols can be short-lived and their reaction can be reversed by chemical reducing agents (*25*). *S*-Nitrosothiol formation could also lead to irreversible oxidative reactions that would permanently activate MMPs. To assess the possibility of these additional oxidative products and further identify the chemical nature of the NO-triggered modification of MMP-9 responsible for activation, we conducted peptide mass fingerprinting (*24*). Mass spectra were obtained after digestion of human R-proMMP-9 with trypsin either in acrylamide gel slices (fig. S4) (*24*) or in solution under native conditions by matrix-assisted laser desorption/ionization time-of-flight (MALDI-TOF) mass spectrometry. Using the latter method, we found a mass peak at 816.7 daltons, representing the propeptide domain fragment CGVPDLGR (*26*) (Fig. 4A, left). We then observed a 48-dalton shift in the mass spectrum of the 816.7-dalton fragment after SNOC exposure, yielding a peak at 864.8 daltons, consistent with oxidation to the sulfonic acid derivative (SO_3H-CGVPDLGR) (Fig. 4A, right; $n = 3$ experiments).

We next asked if the oxidation products of MMP-9 that we encountered in vitro after S-nitrosylation were also present in vivo during focal ischemia and reperfusion. We examined mass spectra of tryptic fragments from affinity-precipitated MMP-9 obtained from rat brain after a 2-hour focal cerebral ischemia and 15-min reperfusion injury or from the contralateral (control) side of the brain ($n = 12$ animals). For these experiments, we performed in-gel digestion with trypsin because gel separation offered better protein resolution. Free cysteines were alkylated to avoid cleavage followed by uncontrolled disulfide formation. MALDI-TOF analysis of specimens obtained from the control side of the brain revealed that after reduction and alkylation by iodoacetamide (57 daltons), the rat propeptide domain fragment (CGVPDVGK, 774 daltons) yielded a peak at 830.3 daltons, representing the alkylated fragment (acet-CGVPDVGK) (Fig. 4B, left). In contrast, on the side of the brain with the stroke, the propeptide domain was not as susceptible to reduction and alkylation, as evidenced by the appearance of an additional peak indicating a propeptide tryptic fragment at 821.8 daltons; this peak represented the addition of a 48-dalton adduct, in accord with sulfonic acid derivatization of the thiol group (SO_3H-CGVPDVGK) (Fig. 4B, right), and was similar to that found in vitro after NO activation of human MMP-9 (Fig. 4A). Additionally, MALDI-TOF mass fingerprinting analysis revealed that, of the 19 cysteine residues present in MMP-9, only the cysteine in the propeptide domain that coordinates Zn^{2+} in the active site was irreversibly modified to a sulfinic ($-SO_2H$) or sulfonic ($-SO_3H$) acid in these experiments (*24*). Our findings indicate that S-nitrosylation of this cysteine residue in the prodomain followed by further oxidation to a sulfinic or sulfonic acid derivative leads to activation of MMP-9. Unlike S-nitrosylation, these latter oxidative reactions are irreversible and therefore contribute to the pathophysiological activation of MMP-9, as found during cerebral ischemia and reperfusion. One of the pathways proposed for oxidation of the nitrosylated cysteine is via hydrolysis to form a sulfenic acid: E-S-N=O + H_2O → E-S-OH + HNO (*25*). The sulfenic acid is labile and susceptible to facile oxidation to the stable sulfinic or sulfonic acid derivatives, as demonstrated by crystal structure modeling (fig. S5) (*24*). Activation of the enzyme can

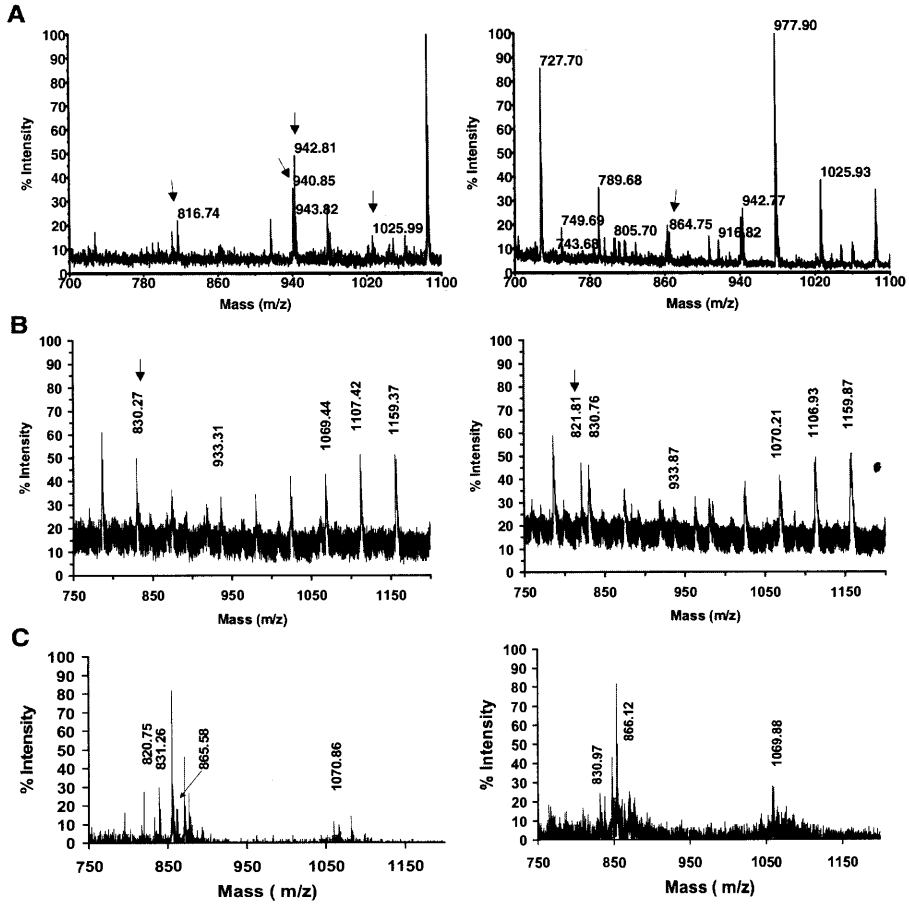

Fig. 4. Peptide mass fingerprinting analysis of the modified thiol group of the cysteine residue within the highly conserved autoinhibitory prodomain of human and rodent MMP-9. (**A**) (Left) MALDI-TOF spectra of in-solution tryptic digest of R-proMMP-9 revealed four signature masses (arrows) from five tryptic fragments. (Right) The tryptic fragment CGVPDLGR at 816.7 daltons shifted by 48 daltons to 864.8 daltons (arrow) after exposure to SNOC, representing SO_3H-CGVPDLGR. (**B**) Detection of tryptic fragments by MALDI-TOF mass spectrometry of gel-purified MMP-9 from rat brains after 2-hour middle cerebral artery (MCA) occlusion plus 15-min reperfusion. MMP-9 was extracted in tris buffer with 1% Triton X-100, affinity precipitated with gelatin Sepharose 4B, subjected to SDS–polyacrylamide gel electrophoresis under nonreducing conditions, and visualized by silver staining. (Left) Gel-purified MMP-9 was reduced and alkylated before digestion. MALDI-TOF mass spectrometry revealed a mass peak at 830.3 daltons (arrow), representing the iodoacetamide (57 daltons)-alkylated rat peptide acet-CGVPDVGK (57 + 774 daltons) from the propeptide domain isolated from control brains. (Right) A mass of 821.8 daltons (arrow), representing the 774-dalton propeptide domain fragment plus a 48-dalton modification (SO_3H-CGVPDVGK), was observed in the ischemic side of the brain. MALDI-TOF spectra did not detect modification of other cysteine residues within MMP-9 tryptic fragments. (**C**) Treatment with 3br7NI before ischemia blocked formation of the sulfinic or sulfonic acid modifications of MMP-9. (Left) In soybean oil vehicle–treated rats, MALDI-TOF mass spectrometry revealed three signature mass peaks of the MMP-9 tryptic fragments (at 831, 866, and 1070 daltons), plus a mass peak of 821 daltons representing the propeptide domain fragment containing a 48-dalton modification (SO_3H-CGVPDVGK). (Right) In rats treated with 3br7NI (30 mg per kg of body weight, intraperitoneal) (*31*), the mass peak at 821 daltons was not detected in the ischemic side of the brain.

occur before cleavage but after sulfinic or sulfonic acid modification, as we were able to observe these derivatives in our peptide analysis of proMMP-9. To confirm the pathophysiological relevance of these findings, we performed the same ischemia and reperfusion experiments after nNOS inhibition with 3br7NI, which is known to be neuroprotective and decrease stroke size. Under these conditions with NO formation blocked, the sulfinic and sulfonic acid oxidation products of activated MMP-9 were not observed in our MALDI-TOF analysis (Fig. 4C). One caveat with these findings is that nNOS deletion or NOS inhibition diminishes stroke damage, and hence one could argue that other stroke-related processes responsible for MMP activation would be reduced. Nonetheless, taken together with the data demonstrating S-nitrosylation of MMPs and our finding that MMPs activated in this manner cause neuronal apoptosis in vitro, it is likely that NO activation of MMPs participates in neuronal injury in vivo.

S-Nitrosylation and subsequent oxidation of protein thiol in the prodomain of MMP-9 can thus lead to enzyme activation, and homologous MMPs may be activated in a similar manner. This series of reactions confers responsiveness of the extracellular matrix to nitrosative and oxidative stress. Such insults are relevant to a number of pathophysiological conditions, including cerebral ischemia and neurodegenerative diseases. Extracellular proteolytic cascades triggered by MMPs can disrupt the extracellular matrix, contribute to cell detachment, and lead to a form of apoptotic cell death known as anoikis, similar to that observed in our neuronal cultures (*27*). The elucidation of an extracellular signaling pathway to neuronal apoptosis involving NO-activated MMPs may contribute to the development of new therapies for stroke and other disorders associated with nitrosative and oxidative stress.

References and Notes

1. V. W. Yong, C. Power, P. Forsyth, D. R. Edwards, *Nature Rev. Neurosci.* **2**, 502 (2001).
2. A. Lukes, S. Mun-Bryce, M. Lukes, G. A. Rosenberg, *Mol. Neurobiol.* **19**, 267 (1999).
3. I. L. Campbell, A. Pagenstecher, *Trends Neurosci.* **22**, 285 (1999).
4. J. Montaner *et al.*, *Stroke* **32**, 1759 (2001).
5. A. M. Romanic, R. F. White, A. J. Arleth, E. H. Ohlstein, F. C. Barone, *Stroke* **29**, 1020 (1998).
6. M. Asahi *et al.*, *J. Cereb. Blood Flow Metab.* **20**, 168 (2000).
7. Y. Gasche *et al.*, *J. Cereb. Blood Flow Metab.* **19**, 1020 (1999).
8. E. Morgunova *et al.*, *Science* **284**, 1667 (1999).
9. H. E. Van Wart, H. Birkedal-Hansen, *Proc. Natl. Acad. Sci. U.S.A.* **87**, 5578 (1990).
10. T. M. Dawson, S. H. Snyder, *J. Neurosci.* **14**, 5147 (1994).
11. S. A. Lipton *et al.*, *Nature* **364**, 626 (1993).
12. G. Melino *et al.*, *Nature* **388**, 432 (1997).
13. J. S. Stamler, *Cell* **78**, 931 (1994).
14. L. Jia, C. Bonaventura, J. Bonaventura, J. S. Stamler, *Nature* **380**, 221 (1996).
15. Y. B. Choi *et al.*, *Nature Neurosci.* **3**, 15 (2000).
16. S. R. Jaffrey, H. Erdjument-Bromage, C. D. Ferris, P. Tempst, S. H. Snyder, *Nature Cell Biol.* **3**, 193 (2001).
17. J. R. Matthews, C. H. Botting, M. Panico, H. R. Morris, R. T. Hay, *Nucleic Acids Res.* **24**, 2236 (1996).
18. S. Sato, T. Tominaga, T. Ohnishi, S. T. Ohnishi, *Brain Res.* **647**, 91 (1994).
19. E. Kumura, H. Kosaka, T. Shiga, T. Yoshimine, T. Hayakawa, *J. Cereb. Blood Flow Metab.* **14**, 487 (1994).
20. J. S. Stamler, E. J. Toone, S. A. Lipton, N. J. Sucher, *Neuron* **18**, 691 (1997).
21. Z. Gu, S. A. Lipton, unpublished observations.
22. Z. Huang *et al.*, *Science* **265**, 1883 (1994).
23. S. J. Kridel *et al.*, *J. Biol. Chem.* **276**, 20572 (2001).
24. Supplementary materials and methods are available on *Science* Online.
25. J. S. Stamler, A. Hausladen, *Nature Struct. Biol.* **5**, 247 (1998).
26. Single-letter abbreviations for the amino acid residues are as follows: A, Ala; C, Cys; D, Asp; E, Glu; F, Phe; G, Gly; H, His; I, Ile; K, Lys; L, Leu; M, Met; N, Asn; P, Pro; Q, Gln; R, Arg; S, Ser; T, Thr; V, Val; W, Trp; and Y, Tyr.
27. M. Cardone, G. S. Salvesen, C. Widmann, G. Johnson, S. M. Frisch, *Cell* **90**, 315 (1997).
28. Y. F. Wang *et al.*, *Nature Med.* **4**, 228 (1998).
29. J. W. Zhang, P. E. Gottschall, *J. Neurosci. Methods* **76**, 15 (1997).
30. S. Z. Lei *et al.*, *Neuron* **8**, 1087 (1992).
31. D. Huang, A. Shenoy, J. Cui, W. Huang, P. K. Liu, *FASEB J.* **14**, 407 (2000).

32. We thank C. Ju for cerebrocortical cultures, G. del Zoppo for helpful discussions, and W. Li and K. Gramatikoff for modeling and illustration of the MMP-9 crystal structure. Z.G. and S.J.K. were supported by NIH grants NRSA T32 AG00252 and AR08505, respectively; M.K. was supported by the American Foundation for AIDS Research; J.W.S., R.C.L., and S.A.L. were supported in part by NIH grants P01 HD29587, R01 EY09024, R01 EY05477, R01 NS41207, R01 AR42750, and R01 CA 69306, and the American Heart Association.

Supporting Online Material

www.sciencemag.org/cgi/content/full/297/5584/1186/DC1.
Methods
Figs. S1 to S5

6 May 2002; accepted 5 July 2002

Myelin-Associated Glycoprotein as a Functional Ligand for the Nogo-66 Receptor

Betty P. Liu, Alyson Fournier, Tadzia GrandPré, Stephen M. Strittmatter*

Axonal regeneration in the adult central nervous system (CNS) is limited by two proteins in myelin, Nogo and myelin-associated glycoprotein (MAG). The receptor for Nogo (NgR) has been identified as an axonal glycosyl-phosphatidylinositol (GPI)–anchored protein, whereas the MAG receptor has remained elusive. Here, we show that MAG binds directly, with high affinity, to NgR. Cleavage of GPI-linked proteins from axons protects growth cones from MAG-induced collapse, and dominant-negative NgR eliminates MAG inhibition of neurite outgrowth. MAG-resistant embryonic neurons are rendered MAG-sensitive by expression of NgR. MAG and Nogo-66 activate NgR independently and serve as redundant NgR ligands that may limit axonal regeneration after CNS injury.

Axons of the adult mammalian CNS possess an extremely limited ability to regenerate after injury, largely because of environmental factors preventing axon growth (*1*, *2*). Characterization of the molecular mechanisms limiting axonal regeneration holds promise for the development of therapeutics to promote recovery after human CNS injury (*3*, *4*). Two factors limiting CNS regeneration, Nogo and MAG, are produced by oligodendrocytes and are distributed in the myelin that ensheathes CNS axons (*5*, *6*). Successful axon regeneration in the peripheral nervous system can be attributed to the absence of Nogo in myelinating Schwann cells, the rapid clearance of MAG by macrophages, and the induction of regeneration-associated genes (*1*–*6*). The recently identified Nogo receptor (NgR) is a leucine-rich repeat (LRR) protein that is GPI-anchored to the outer leaflet of the plasma membrane and binds a discrete cell-surface Nogo domain, Nogo-66 (*7*). MAG is recognized as a sialic acid–binding SIGLEC (sialic acid–dependent immunoglobulin-like family member lectin) protein with an affinity for gangliosides GD1a and GT1b (*8*–*14*). It has been suggested that these gangliosides might serve as axonal MAG receptors (*11*). No axonal proteins with high affinity for MAG have been identified. Here, we find that NgR serves as a receptor for MAG as well as Nogo-66, indicating that blockade of this one receptor may reverse the action of two inhibitors of CNS axonal regeneration.

NgR lacks an intracellular component, suggesting that it serves as the primary Nogo-66 binding site while an associated transmembrane coreceptor subunit mediates intracellular signal transduction (*7*). We sought to identify a coreceptor component by using an expression-cloning strategy based on the binding of a soluble fusion protein composed

Department of Neurology and Section of Neurobiology, Yale University School of Medicine, New Haven, CT 06510, USA.

*To whom correspondence should be addressed. E-mail: stephen.strittmatter@yale.edu